

Gluon propagators in $2 + 1$ lattice QCD with nonzero isospin chemical potential

V. G. Bornyakov

*NRC “Kurchatov Institute”– IHEP Protvino, 142281, Russian Federation,
NRC “Kurchatov Institute”– ITEP, Moscow 117218, Russian Federation,
School of Biomedicine, Far Eastern Federal University,
Sukhanova 8, Vladivostok, 690950, Russian Federation*

A. A. Nikolaev

Department of Physics, College of Science, Swansea University, Swansea SA2 8PP, United Kingdom

R. N. Rogalyov

NRC “Kurchatov Institute”– IHEP Protvino, 142281, Russian Federation

A. S. Terentev

National University of Science and Technology “MISIS”, Leninsky Avenue 4, 119991 Moscow, Russia

The static longitudinal and transverse gluon propagators in the Landau gauge are studied in $2 + 1$ lattice QCD with nonzero isospin chemical potential μ_I . Parameterization of the momentum dependence of the propagators is provided for all values of the chemical potential under study. We find that the longitudinal propagator is infrared suppressed at nonzero μ_I with suppression increasing with increasing μ_I . It is found, respectively, that the electric screening mass is increasing with increasing μ_I . Additionally, we analyze the difference between two propagators as a function of the momentum and thus compare interactions in chromoelectric and chromomagnetic sectors.

PACS numbers: 11.15.Ha, 12.38.Gc, 12.38.Aw
Keywords: gauge field theory, gluon propagator

I. INTRODUCTION

To understand the physics of neutron star matter and results of heavy-ion collision experiments it is important to study the quark matter with isospin (isotopic) asymmetry. QCD phase diagram at nonzero values of the isospin chemical potential μ_I has been studied recently quite intensively using lattice QCD [1–11], effective models as NJL model [12–20], quark meson model [21–23], chiral perturbation theory [24–26], perturbative QCD [27, 28], random matrix model [29], hadron resonance gas model [30] and other approaches, see e.g. recent review [31].

It is also believed that the study of QCD at nonzero μ_I might help, in one way or another, to solve more difficult problem of QCD at nonzero baryon chemical potential. First, QCD with nonzero μ_I is an ideal test system for some lattice approaches to QCD with nonzero baryon chemical potential such as Taylor expansion, analytical continuation and others. Second, lattice results obtained at nonzero μ_I by means of first principle calculations can be compared with respective results of the effective field theories of QCD and phenomenological models. Such comparison allows to test the effectiveness of QCD models and thus to estimate their applicability to the study of QCD at nonzero μ_B .

The gluon propagators are among important quantities to study. Contemporary perturbative computations of the equation of state of high-density strong-interacting

matter employ infrared behavior of gluon propagators described in terms of screening (see, e.g. [32] and references therein). Nonperturbative estimates of such screening effects on the basis of lattice simulations may be used for testing the methods of resummation of perturbation series.

In early calculations of pressure at nonzero quark chemical potentials [33], the full gluon propagators appear in the expressions for the thermodynamical potential $\Omega(T, V, \mu)$. If the Green functions that appear in such expressions were evaluated nonperturbatively, the dynamics of pressure build-up and other thermodynamic quantities could be investigated in detail.

The gluon propagator results also will be useful in testing future results obtained at nonzero μ_I by the functional methods like Dyson-Schwinger equation and functional renormalization group.

Landau gauge gluon propagators in the non-Abelian gauge theories at zero and nonzero temperature were extensively studied in the infrared range of momenta by various methods. We shall note lattice gauge theory, Dyson-Schwinger equations, Gribov-Zwanziger approach. At the same time the studies at nonzero quark chemical potential are restricted to a few papers only. Here we close this gap for the case of nonzero isospin chemical potential. Let us note that for the lattice QCD at nonzero baryon chemical potential the results can be obtained only for small values of μ_B because of the sign problem [34].

It is known that in QCD with nonzero μ_I there is a phase transition from the normal to the superfluid phase at $\mu_I = \mu_\pi/2$. Recently results were obtained [10] indicating that at large μ_I the theory undergoes smooth transition to the deconfinement phase. It is interesting to check if the gluon propagators change at respective values of μ_I .

In this paper we make the first study of the influence of μ_I on the Landau gauge gluon propagators using lattice QCD approach. We use the same lattice action as in Ref. [10] and in fact the same set of the lattice configurations. Our goal is to study how the gluon propagators change with an increase of μ_I . In particular, we find strong suppression of the (color)-electric (longitudinal) gluon propagator with increasing μ_I which is reflected in increasing of the respective screening mass. We parameterize the propagators in the wide range of momentum values using the fit function which is the tree level prediction of the Refined Gribov-Zwanziger approach. We also compute an observable introduced recently in [35], a difference between the (color)-electric and (color)-magnetic propagators, and obtain its dependence on the momentum and isospin chemical potential.

The paper is organized as follows. In Section II we specify details of the lattice setup to be used: lattice action, definition of the propagators and details of the simulation. In Section III we consider the propagators at low momenta to compute respective screening masses and determine their dependence on μ_I . In Section IV the fit over a wide range of momenta is performed using Gribov-Stingl fit function motivated by the Refined Gribov-Zwanziger effective action. We demonstrate that for the longitudinal propagator this fit works well over the whole momenta domain under study for all values of μ_I considered, whereas for the transverse propagator it works only at small μ_I .

In Section V the dependence of the difference between the electric and magnetic propagators on the momentum and isospin chemical potential is discussed. We show that this difference decreases exponentially fast with momenta similarly to the case of $SU(2)$ QCD [35]. The last section is devoted to the discussion of the results and to conclusions to be drawn.

II. SIMULATION DETAILS

We carry out our study of the 2 + 1 lattice QCD with light quark mass $m_u = m_d \equiv m_{ud}$ and strange quark mass m_s using 28^4 lattices for a set of the chemical potentials in the range $a\mu_I \in (0, 0.42)$. The tree level improved Symanzik gauge action [36] and the staggered fermion action with a pion source term were used to generate the lattice gauge field configurations [10].

The partition function (after integration over the quark fields) is of the form [7–10]

$$Z = \int DU e^{-S_G(U)} \det[M_{ud}^\dagger M_{ud} + \lambda^2]^{1/4} \det[M_s]^{1/4} \quad (1)$$

where λ is coupling of the pionic source term, light quarks lattice operator M_{ud} and strange quark lattice operator M_s are

$$M_{ud} = \not{D}(\mu_I) + m_{ud}, \quad M_s = \not{D}(0) + m_s, \quad (2)$$

$\not{D}(\mu_I)$ is the staggered lattice Dirac operator with quark chemical potential $\mu_I = \mu_u = -\mu_d$. The unphysical pionic source term which breaks $U(1)$ symmetry explicitly is necessary to observe the spontaneous breaking of this symmetry in a finite volume in the limit $\lambda \rightarrow 0$ at high enough μ_I [1]. The lattice configurations were generated [10] at $\beta = 4.036$, $am_{ud} = 0.0077$, $am_s = 0.0271$, $\lambda = 0.5am_{ud}$. The lattice spacing of the ensemble in physical units was determined via the Sommer scale value $r_0 = 0.468$ fm [37] to be $a = 0.0687$ fm. Then the pion mass in physical units is $m_\pi = 380$ MeV [10].

Our lattice spacing is small enough to be sure that usual lattice discretization effects are small. However, at nonzero isospin chemical potential new lattice artifacts may appear. To reach large quark densities without lattice artifacts one needs sufficiently small lattice spacing to satisfy condition $a\mu_I \ll 1$. Actual values of $a\mu_I$ under consideration are given in Table I of Appendix A, one can see that $a\mu_I < 0.42$. Thus we can hope that respective lattice artifacts are small.

At the same time to study the gluon propagators in the infrared region it is necessary to employ large physical volume. As a result of a compromise between these two requirements our lattice size is rather moderate: $L = 28a = 1.92$ fm. This implies a potential problem of large finite volume effects at small momenta (the minimal momentum $p_{min} \approx 650$ MeV).

Our lattice with equal number of temporal and spatial sites $N_s = N_t = 28$ corresponds to the temperature $T = \frac{1}{28a} \approx 100$ MeV. However, the energy of the lightest excitation at $\mu_I = 0$ is estimated as $E_{exc} \geq p_{min} = 650$ MeV. Since $E_{exc} \gg T$, this temperature can be considered as approximately zero. At the greatest isospin chemical potential under study, $\mu_I = 1.2$ GeV, the energy of the lightest excitation can be estimated as follows. Using the model of free quarks, we notice that in the respective ground state all modes with $|\vec{p}| < \mu_I$ are occupied by $u\bar{d}$ quark states (27 modes with $|\vec{p}| \leq p_{min}\sqrt{3}$ in the case under consideration). The lightest excitation occurs when one light quark jumps from the mode with $|\vec{p}| = p_{min}\sqrt{3}$ to the mode with $|\vec{p}| = 2p_{min}$. The energy needed for this purpose is $E_{exc} \sim 170$ MeV, therefore, in a rough approximation, the temperature $T \sim 100$ MeV can be thought of as zero even at $\mu_I = 1.2$ GeV.

In our study of the gluon propagators we employ the standard definition of the lattice gauge vector potential $A_{x,\mu}$ [38]:

$$A_{x,\mu} = \frac{1}{2ia g} \left(U_{x\mu} - U_{x\mu}^\dagger \right) \Big|_{\text{traceless}}. \quad (3)$$

The lattice Landau gauge fixing condition is

$$(\nabla^B A)_x \equiv \frac{1}{a} \sum_{\mu=1}^4 (A_{x,\mu} - A_{x-a\hat{\mu},\mu}) = 0, \quad (4)$$

which is equivalent to finding an extremum of the gauge functional

$$F_U(\omega) = \frac{1}{4V} \sum_{x,\mu} \frac{1}{3} \text{Re Tr } U_{x\mu}^\omega, \quad (5)$$

with respect to gauge transformations ω_x . To fix the Landau gauge we use the simulated annealing (SA) algorithm with finalizing overrelaxation [39, 40].

The gluon propagator $D_{\mu\nu}^{ab}(p)$ is defined as follows:

$$D_{\mu\nu}^{ab}(p) = \frac{T}{V} \langle \tilde{A}_\mu^a(q) \tilde{A}_\nu^b(-q) \rangle, \quad (6)$$

where $V = (N_s a)^3$, $T = \frac{1}{N_t a}$,

$$\begin{aligned} \tilde{A}_\mu^b(q) = a^4 \sum_x A_{x,\mu}^b \exp & \left(\frac{2\pi i q_4}{N_t} \left(\frac{x_4}{a} + \frac{\delta_{\mu 4}}{2} \right) \right) \\ & + \frac{2\pi i q_k}{N_s} \left(\frac{x_k}{a} + \frac{\delta_{\mu k}}{2} \right), \end{aligned} \quad (7)$$

$q_i \in (-N_s/2, N_s/2]$, $q_4 \in (-N_t/2, N_t/2]$ and the physical momenta p_μ are defined by the relations $ap_i = 2 \sin(\pi q_i/N_s)$, $ap_4 = 2 \sin(\pi q_4/N_t)$; $p = \sqrt{\sum_{\mu=1}^4 p_\mu^2}$.

At nonzero μ_I the $O(4)$ symmetry is broken and there are two tensor structures for the gluon propagator [41]:

$$D_{\mu\nu}^{ab}(p) = \delta_{ab} (P_{\mu\nu}^T(p) D_T(p) + P_{\mu\nu}^L(p) D_L(p)), \quad (8)$$

where (symmetric) orthogonal projectors $P_{\mu\nu}^{T;L}(p)$ are defined for $p = (\vec{p} \neq 0; p_4 = 0)$ as follows

$$P_{ij}^T(p) = \left(\delta_{ij} - \frac{p_i p_j}{p^2} \right), \quad P_{\mu 4}^T(p) = 0; \quad (9)$$

$$P_{44}^L(p) = 1; \quad P_{\mu i}^L(p) = 0. \quad (10)$$

Therefore, two scalar propagators - longitudinal $D_L(p)$ and transverse $D_T(p)$ - are given by

$$D_T(p) = \frac{1}{16} \sum_{a=1}^8 \sum_{i=1}^3 D_{ii}^{aa}(p); \quad (11)$$

$$D_L(p) = \frac{1}{8} \sum_{a=1}^8 D_{44}^{aa}(p). \quad (12)$$

For $\vec{p} = 0$ they are defined as follows:

$$D_T(0) = \frac{1}{24} \sum_{a=1}^8 \sum_{i=1}^3 D_{ii}^{aa}(0), \quad (13)$$

$$D_L(0) = \frac{1}{8} \sum_{a=1}^8 D_{00}^{aa}(0). \quad (14)$$

$D_T(p)$ is associated with the magnetic sector, $D_L(p)$ - with the electric sector. We consider the soft modes $p_4 = 0$ and use the notation $D_{L,T}(p) = D_{L,T}(0, |\vec{p}|)$.

III. SCREENING MASSES

Various definitions of the screening masses were discussed in great detail in our previous studies [35, 42]. Here we use the definition in terms of the Taylor expansion of $D_{L,T}^{-1}(p)$ in p^2 at low momenta:

$$D_{L,T}^{-1}(p) = Z^{-1} (\tilde{m}_{E,M}^2 + p^2 + c_4 \cdot (p^2)^2 + c_6 (p^2)^3 \dots). \quad (15)$$

This method was used in [43] in the studies of lattice QCD at finite temperature and was applied to QC₂D in [42]. One can note that the Yukawa-type fit-function

$$D_{L,T}^{-1}(p) = Z^{-1} (\tilde{m}_{E,M}^2 + p^2) \quad (16)$$

successfully employed in the previous studies of lattice gluodynamics at zero and finite temperatures in Refs.[44–46] does not work in the case under consideration because the minimal nonzero momentum on our lattices is rather large: $p_{\min} \approx 640$ MeV. Thus we have no data points in deep infrared domain, where higher-order terms in formula (15) can be neglected. As explained below, we have to take into account up to the $\underline{O}((p^2)^3)$ terms of the Taylor expansion of the inverse propagators.

It should be noted that the screening masses $\tilde{m}_{E,M}^2$ are related to the correlation lengths:

$$\tilde{m}_{E,M}^2 = \xi_{E,M}^{-2}, \quad (17)$$

where $\xi_{E,M}$ are usually defined in terms of propagators as follows [47]:

$$\begin{aligned} \xi^2 &= \frac{1}{2} \frac{\int_V dx_4 d\vec{x} D(x_4, \vec{x}) |\vec{x}|^2}{\int_V dx_4 d\vec{x} D(x_4, \vec{x})} \\ &= -\frac{1}{2D(0, \vec{0})} \sum_{i=1}^3 \left(\frac{d}{dp_i} \right)^2 \Big|_{\vec{p}=0} D(0, \vec{p}). \end{aligned} \quad (18)$$

To extract the screening masses from the data, we employ the fit function (15) keeping terms up to p^2 or $(p^2)^2$ or $(p^2)^3$, depending on the fit range. We will call below respective fit functions as fit function with two terms, with three terms or with four terms. We perform the fit over the range $p_{\text{low}} \leq p < p_{\text{cut}}$, where p_{low} is equal to either zero or p_{\min} and p_{cut} varies from 1.3 GeV to 2 GeV.

We find that, in the general case, both m_E and m_M depend substantially on the choice of p_{low} , p_{cut} and the fit function. To improve stability of the results, we consider the propagators as functions of 2 variables, $D_{L,T}^{-1}(p, \mu_I)$. In so doing, we assume smooth dependence of a propagator on both variables and fit the overall set of data by a polynomial in p^2 and μ_I^2 thus reducing drastically the

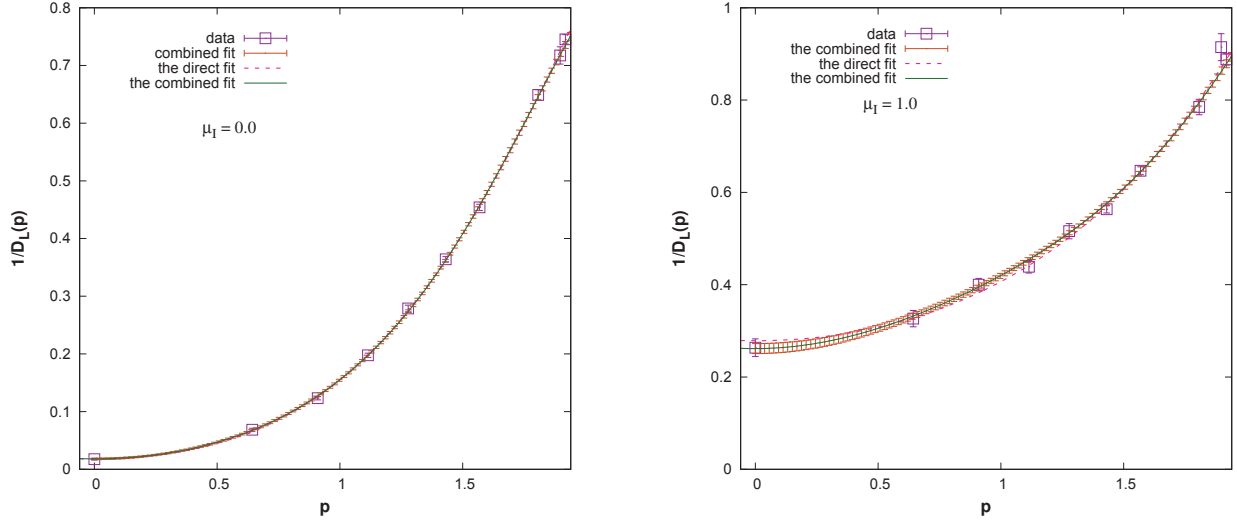


FIG. 1: The inverse longitudinal propagator interpolated by formula (20) (the combined fit) or by (15) (the direct fit) at $\mu_I = 0$ (left panel) and $\mu_I = 1$ GeV (right panel). The corridors of errors in the former case are shown by the respective error bars. Data are shown by purple squares.

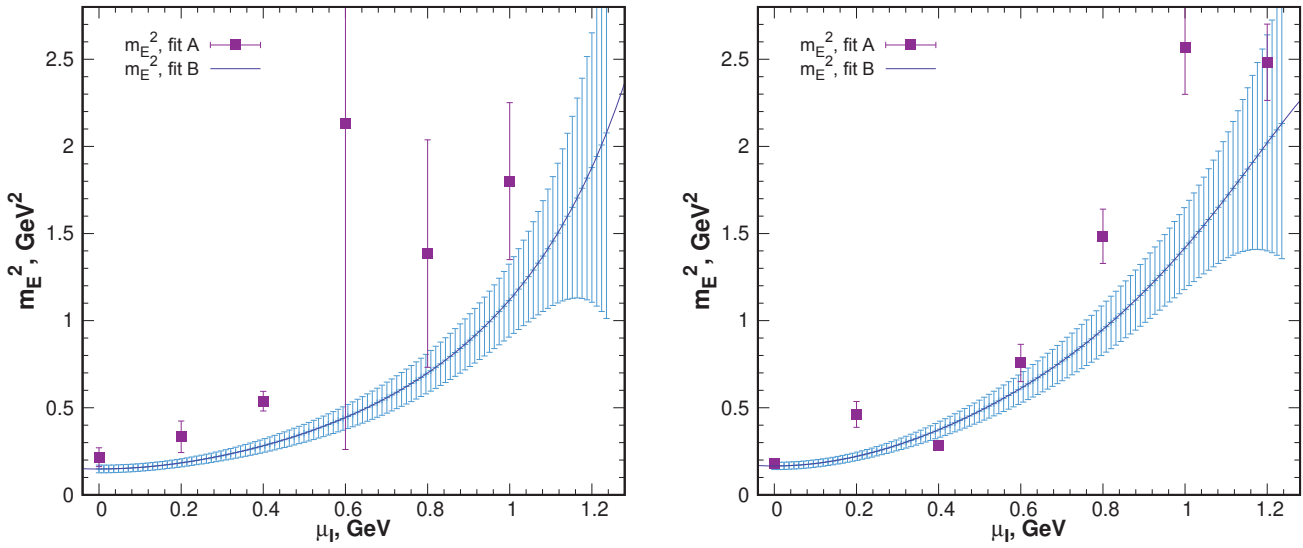


FIG. 2: The chromoelectric squared screening masses as a function of the isospin chemical potential. Fit A is related to the fit functions (15); fit B—to (20); the momentum ranges are $0 \leq p < 1.5$ GeV (left) and $0 \leq p < 2$ GeV (right). Curves show interpolated values of the screening masses evaluated by the formula (21), the respective corridors of errors are shown by error bars.

total number of estimated parameters. We choose the polynomial by selecting a finite number of terms in the series

$$D_{L,T}^{-1}(p, \mu_I) \simeq \sum_{n=0}^{\infty} \sum_{k=0}^{\infty} c_{2n,2k} (p^2)^n \mu_I^{2k}, \quad (19)$$

we omit the superscript L or T of the coefficients $c_{i,j}$.

Odd powers of μ_I are prohibited by isospin symmetry of strong interactions and, in particular, gluon propagators are invariant under the change $\mu_I \rightarrow -\mu_I$. Such polynomials providing a reliable quality of the fit are found by trial-and-error method in the longitudinal case, the resulting expressions for each fit range are given below. The results of this (that is, combined) and the direct (that is, by formulas like (15)) fits for the inverse prop-

agator at a given value of μ_I are compared in Fig. 1. It should be remembered that an increase of the number of estimated parameters gives rise to increasing of uncertainties in their values, whereas a decrease of this number results in either a dramatic decrease of the fit p -value or in a substantial shrinking of the fit range.

In the case of transverse propagator both fitting procedures are not stable with respect to elimination of the zero momentum; data on larger lattices and increased statistics are needed to arrive at reliable results. In this study, screening in the magnetic sector is discussed in terms of the dressing function, see Section V.

A. Chromoelectric screening mass

We fit our data by the function (15) with three or four terms using $p_{\text{cut}} = 1.3, 1.5$ or 2.0 GeV and $p_{\text{low}} = 0$ or p_{min} . The results of the fits are stable with respect to exclusion of the zero momentum only for $p_{\text{cut}} = 2$ GeV. In this case, the fit function (15) with three terms works well at $\mu_I \geq 0.4$ GeV; at $0 \leq \mu_I \leq 0.2$ GeV we employ the fit function (15) with four terms. These results are shown in the right panel of Fig. 2 by squares. In performing this fitting procedure we determine in total 23 fit parameters (when all values of μ_I are taken into account).

As we explained above one can substantially reduce the number of fit parameters by considering the inverse propagator as function of p and μ_I . This approach also makes it possible to derive m_E^2 as function of μ_I and estimate respective confidence interval for each value of $\mu_I \in (0, 1.2$ GeV).

An appropriate goodness of fit ($\chi^2/34 = 1.66$, p -value ≈ 0.009) can be achieved for the momentum range $0 \leq p < 1.5$ GeV with the following 15-parameter fit function

$$D_L^{-1}(p, \mu_I) \simeq c_{00} + c_{02}\mu_I^2 + c_{04}\mu_I^4 + c_{06}\mu_I^6 \quad (20)$$

$$+ c_{20}p^2 + c_{22}p^2\mu_I^2 + c_{24}p^2\mu_I^4 + c_{26}p^2\mu_I^6$$

$$+ c_{40}p^4 + c_{42}p^4\mu_I^2 + c_{44}p^4\mu_I^4$$

$$+ c_{60}p^6 + c_{62}p^6\mu_I^2 + c_{64}p^6\mu_I^4 + c_{80}p^8.$$

The same fit function provides the best fit quality ($\chi^2/27 = 1.20$, p -value ≈ 0.22) when the data at $p = 0$ are excluded: $p_{\text{min}} < p < 1.5$ GeV, $0 \leq \mu_I \leq 1.2$ GeV. An increase of p_{cut} to 2 GeV results in some decrease of the p -value ($\chi^2/55 = 1.55$, p -value ≈ 0.005).

The square of the chromoelectric screening mass is then determined by the expression

$$m_E^2(\mu_I) = \frac{c_{00} + c_{02}\mu_I^2 + c_{04}\mu_I^4 + c_{06}\mu_I^6}{c_{20} + c_{22}\mu_I^2 + c_{24}\mu_I^4 + c_{26}\mu_I^6} \quad (21)$$

The error in this quantity which takes into account the correlations between the fit parameters was calculated with the use of the REDUCE computer algebra system.

The respective corridor of errors is shown by the error bars in Fig.2.

It should be emphasized that the fit (20) (fit B) at both values of p_{cut} and the fit (15) (fit A) at $p_{\text{cut}} = 2.0$ GeV are stable with respect to an exclusion of $p = 0$ data. This indicates that the dynamics below p_{min} has only a little effect on the screening in the chromoelectric sector.

We show the results of fit A (15) with huge errors (for $p_{\text{cut}} = 1.5$ GeV) in the left panel of Fig.2 in order to illustrate the advantages of fit B (20). Some disagreement between the results of the fit A and B is observed, especially in the right panel of Fig.2 at $\mu_I \sim 1.0$ GeV ($p_{\text{cut}} = 2.0$ GeV). It should be emphasized that, in performing fit A, the term $\sim p^8$ is not taken into account when $p_{\text{cut}} = 2.0$ GeV and the terms $\sim p^6$ and $\sim p^8$ are not taken into account when $p_{\text{cut}} = 1.5$ GeV, whereas all these terms are included in fit function (20) in both cases. The mentioned disagreement indicates that these terms play a significant role at $p > 1$ GeV. In view of this facts we conclude that the results obtained with fit B are more reliable provided that m_E^2 is a smooth function of μ_I . The systematic error of fit B can be estimated by a comparison of the error corridors for the cutoff momenta $p_{\text{cut}} = 1.5$ GeV and $p_{\text{cut}} = 2.0$ GeV as well as the error corridor for the case when the zero momentum is eliminated. It is smaller than the statistical error.

One can see in Fig.2 that the chromoelectric screening mass remains approximately constant at $0 \leq \mu_I \leq 0.4$ GeV and increases with μ_I at its greater values. The dependence of m_E on μ_I found here is qualitatively similar to its dependence on the temperature at $T > T_c$ both in pure gluodynamics and QCD as was demonstrated by lattice simulations in [44, 46]. It is also similar to the dependence of m_E on the baryon chemical potential in QC_2D [35, 42].

Recollecting the dependence of m_E and m_M on μ_q and T in QC_2D obtained in [48], one is tempted to assume that the screening in the magnetic sector will increase with T starting from $T \sim 200 \div 300$ MeV at all values of μ_I , whereas m_E will show a pronounced increase only at small values of μ_I . Testing this hypothesis should be the subject of future studies.

IV. DEPENDENCE ON THE MOMENTUM AND ISOSPIN CHEMICAL POTENTIAL

First we consider the momentum dependence of the gluon propagators for various values of μ_I in more detail. The propagators are renormalized according to the MOM scheme to satisfy the condition

$$D_{L,T}(p = \kappa) = 1/\kappa^2 \quad (22)$$

at $\kappa = 3$ GeV.

In Fig 3 (left) we present the momentum dependence for the longitudinal propagator $D_L(p)$ for some values of μ_I . In the infrared domain it clearly decreases with

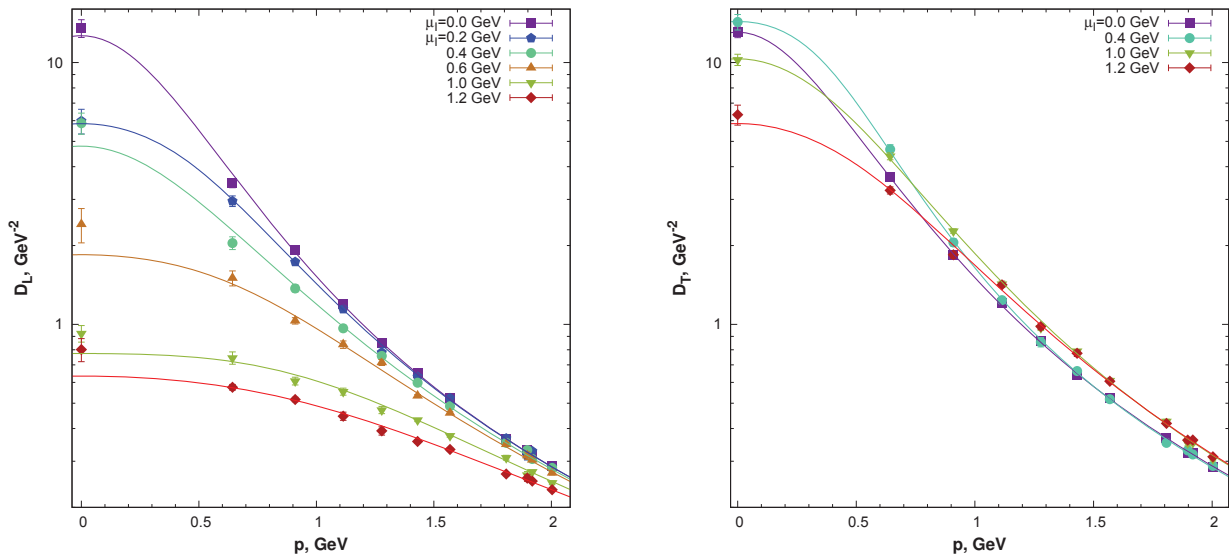


FIG. 3: The propagators D_L (left) and D_T (right) as functions of p at different values of μ_I . The curves correspond to the formula (23).

an increase of μ_I . This dependence on μ_I is similar to the dependence of $D_L(p)$ on T at $T > T_c$ in both gluodynamics and QCD [49–51] as well as on μ_q in QC₂D [35].

In Fig. 3(right) the momentum dependence for the transverse propagator $D_T(p)$ for the same values of μ_I is shown. It is clearly seen that $D_T(p)$ is substantially less sensitive to an increase of μ_I . In the deep infrared region μ_I dependence of the transverse propagator differs substantially from that of the longitudinal propagator. It increases with μ_I at small μ_I until it reaches a weakly pronounced peak (at $\mu_I \simeq 0.4$ GeV for $0 \leq p \leq 0.6$ GeV and at $\mu_I \simeq 0.8$ GeV at $p = 0.9$ GeV, see also Fig.4) and then it gradually decreases. At $p > 1$ GeV the transverse propagator increases at intermediate values of μ_I : $0.4 \leq \mu_I \leq 0.8$ GeV and remains approximately constant at both low and high values of μ_I . A typical dependence of this type is shown in Fig.4 (right panel) by purple triangles; this behavior is also in contrast to that of the longitudinal propagator, which decreases with μ_I at all momenta as is seen in the left panel of Fig. 4

It is known that at a finite temperature the propagator $D_T(p)$ has a clear maximum at the value of momentum increasing with temperature. Our data give no evidence for such maximum at a small momentum, however, we do not rule out its existence.

Now we proceed to an interpolation formula for our data. It was demonstrated many times [51–55] that the infrared behavior of the gluon propagators at zero and finite temperature can be well described by the fit function proposed in [57] as well as the tree level prediction

of the Refined Gribov-Zwanziger approach [58],

$$D(p) = Z \frac{M_1^2 + p^2}{p^4 + M_2^2 p^2 + M_3^4}. \quad (23)$$

This fit function is in fact identical to that used in our previous study [35], the relations between the two sets of fit parameters are obvious.

Since the minimal nonzero momentum p_{\min} for the lattice under study is rather large our fit over the infrared domain may suffer from finite-volume effects. Nevertheless, we believe that we find qualitatively correct dependence of the propagators on μ_I , at least for D_L at large μ_I .

To lower uncertainties in the fit parameters M_i , we perform fit for the ratio

$$\frac{D(p)}{D(p_0)} \simeq \frac{M_1^2 + p^2}{p^4 + M_2^2 p^2 + M_3^4} \frac{p_0^4 + M_2^2 p_0^2 + M_3^4}{M_1^2 + p_0^2}. \quad (24)$$

where p_0 should lie in the fit domain; our choice is $p_0 = 2$ GeV. In so doing, the normalization factors $Z_{L,T}$ are not determined and thus should be computed by the formula

$$Z = \frac{\kappa^4 + M_2^2 \kappa^2 + M_3^4}{\kappa^2 (M_1^2 + \kappa^2)}. \quad (25)$$

With this Z factor, formula (23) gives the propagator renormalized at $p = \kappa$.

The fit domain in the longitudinal case ranges up to $p_{\text{cut}} = 5$ GeV; in the transverse case the cutoff momentum for each value of μ_I is indicated in Table II.

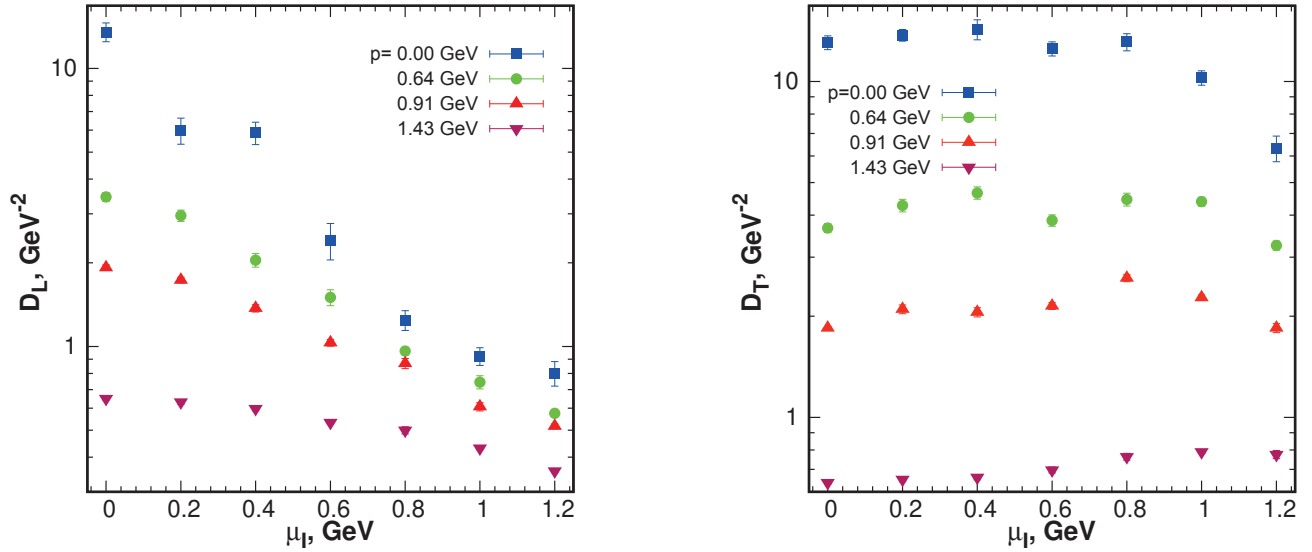


FIG. 4: The propagators D_L (left) and D_T (right) as functions of μ_I at different values of p . Note logarithm scale on the y axis.

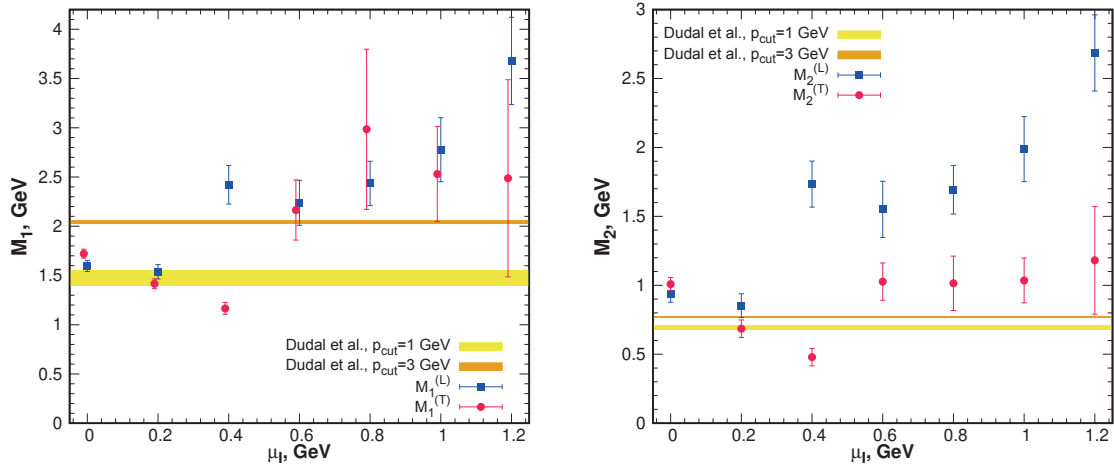


FIG. 5: Parameters M_1 (left) and M_2 (right) of the fit (23) as functions of μ_I . Yellow strips show the results obtained in [55] with $p_{\text{cut}} = 1$ GeV, brown strips—with $p_{\text{cut}} = 3$ GeV.

A few words about the fit stability should be said. In the longitudinal case, the fit parameters are unaffected by elimination of zero momentum, in the transverse case the fit parameters change significantly at 4 of 7 values of μ_I when zero momentum is excluded.

The fit parameters for $D_L(p)$ depend only weakly on the cutoff momentum, as is shown, as an example, in Table III for $\mu_I = 0$; the range $2.2\text{GeV} < p_{\text{cut}} < 5.0$ GeV is considered (at lower value of p_{cut} the fit parameters are poorly determined). At the other values of μ_I the p_{cut} -dependence of M_i is also insignificant, however, the minimum value of p_{cut} at which the fit parameters can

be determined increases with μ_I and reaches 4.5 GeV at $\mu_I = 1.2$ GeV.

The fit parameters and goodness-of-fit for $D_T(p)$ depend on p_{cut} as follows. At $\mu_I = 0.0$ and 0.2 GeV we arrive at a reasonable p -value for $1.9 < p_{\text{cut}} < 5.0$ GeV, M_i depend on p_{cut} only weakly. At $\mu_I = 0.4$ GeV, a reasonable p -value for $1.9 < p_{\text{cut}} < 5.0$ GeV also holds, however, M_i depend significantly on p_{cut} at $p_{\text{cut}} > 3$ GeV. At $0.6 \leq \mu_I \leq 1.2$ GeV we obtain p -value ≥ 0.05 only at $p_{\text{cut}} \leq 2.2$ GeV (this one can see in Fig. 7(right) for the transverse dressing function). At $1.9 \leq p_{\text{cut}} \leq 2.2$ GeV M_i vary within their errors and at $p_{\text{cut}} \leq 1.9$ GeV they

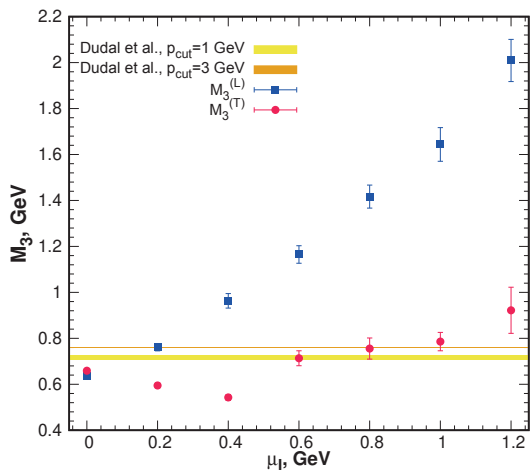


FIG. 6: Parameter M_3 of the GS fit (23) as a function of μ_I . Yellow strip shows the result obtained in [55] with $p_{\text{cut}} = 1$ GeV, brown strip—with $p_{\text{cut}} = 3$ GeV.

are poorly determined.

The parameters of this fit are presented in tables I and II for the longitudinal and transverse propagators, respectively. The parameters M_1^2 , M_2^2 , and M_3^4 are given in the respective powers of GeV for the sake of comparison with [55]. Results of this fit are also shown in Fig. 3 together with our lattice data.

The dependence of these fit parameters on the isospin chemical potential is presented in Figs. 5 and 6, where our results are compared with those obtained in [55] in $SU(3)$ gluodynamics at $T = 0$ on a large lattice with high statistical precision.

The parameters $M_1^{(L)}$ and $M_2^{(L)}$ have a similar dependence on μ_I : they jump between $\mu_I = 0.2$ and 0.4 GeV and slowly increase at $\mu_I > 0.6$ GeV; the parameter $M_3^{(L)}$ shows approximately linear growth through the whole range μ_I under consideration.

In the case of the transverse propagator all $M_i^{(T)}$ approach a shallow minimum at $\mu_I \approx 0.4$ GeV and remain constant (within error bars) at $\mu_I > 0.6$ GeV. A pronounced difference between $M_i^{(L)}$ and $M_i^{(T)}$ is seen at $\mu_I = 0.4$ GeV, this may be caused by the transition from the normal to the superfluid phase which is expected at $\mu_I \sim 0.2$ GeV.

It is instructive to look also at the respective dressing functions $J_{L,T}(p)$ defined as

$$J_{L,T}(p) = p^2 D_{L,T}(p) \quad (26)$$

It is seen in Figure 7 (left) that with increasing μ_I the maximum of the longitudinal dressing function goes down and shifts to the right, thus approaching dressing function of a massive scalar particle. We note once more that this dependence on μ_I is very similar to dependence on the temperature, see e.g. Ref. [50, 56].

The transverse dressing function increases at $\mu_I < 0.8$ GeV so that it approaches its peak at $p \sim 0.7 \div$

0.9 GeV, at larger μ_I the height of the peak decreases with increasing μ_I and the position shifts to $p \sim 1.0 \div 1.1$ GeV.

The difference between the transverse and longitudinal dressing functions $\Delta J = J_T - J_L$ is shown in Fig. 8, right panel. It equals zero at $\mu_I = 0$ and then it rapidly increases over the range $0 < \mu_I < 0.4$ GeV. Then, as μ_I increases from 0.4 to 1.2 GeV, the height of its peak fluctuates over $0.8 < \Delta J < 1.1$, the width increases and the position shifts to higher values of p .

It should be emphasized that, at $0 < \mu_I < 0.4$ GeV, when both screening masses remain constant, ΔJ shows a rapid change.

V. FEATURES OF $D_L - D_T$ BEHAVIOR

In the previous two sections we demonstrated that the difference between the longitudinal and transverse propagators increases with an increase of the isospin chemical potential. Therewith, they come close to each other at high momenta for a fixed value of μ_I . In this section we study the rate of the decrease of $\Delta(p) = D_T(p) - D_L(p)$ with increasing momentum and how the picture changes with increasing μ_I . A similar comparison of these two propagators was made in [35] in QC_2D as well as in [46] in $SU(3)$ gluodynamics at finite temperatures where the ratio $D_L(p)/D_T(p)$ was considered.

Here we show that, in the theory under study, the difference between transverse and longitudinal propagators, $\Delta(p) = D_T(p) - D_L(p)$ at $p_4 = 0$ shows clear exponential dependence on p .

Our numerical results for $\Delta(p)$ are presented in Fig. 8 (left), together with the fit function

$$\Delta(p) = c \exp(-\nu \cdot p). \quad (27)$$

The exponential decreasing is well established starting from some momentum p_0 depending on μ_I . We found that $0 < p_0 < p_{\text{min}}$ for $0.2 \leq \mu_I \leq 1.0$ GeV and $p_0 \approx 1.2$ GeV for $\mu_I = 1.2$ GeV. The upper limit of the fit domain $p_0 < p < p_{\text{cut}}$ is determined by the requirement that $\Delta(p)$ differs from zero by more than 3 statistical errors (see Table IV).

As a check we compare the fit function (27) with the power fit function

$$\Delta(p) = \frac{C}{p^v} \quad (28)$$

motivated by a power-like behavior of both gluon propagators when $p \rightarrow \infty$.

At $0.2 \leq \mu_I \leq 0.4$ both fit functions work well because $\Delta(p)$ does not vanish for only a few momenta. At $\mu_I > 0.4$ GeV only the exponential fit function (27) works. Moreover, we strengthen this conclusion by considering three-parameter power-like fit function as follows:

$$\Delta(p) \simeq \frac{C}{(p+d)^v}; \quad (29)$$

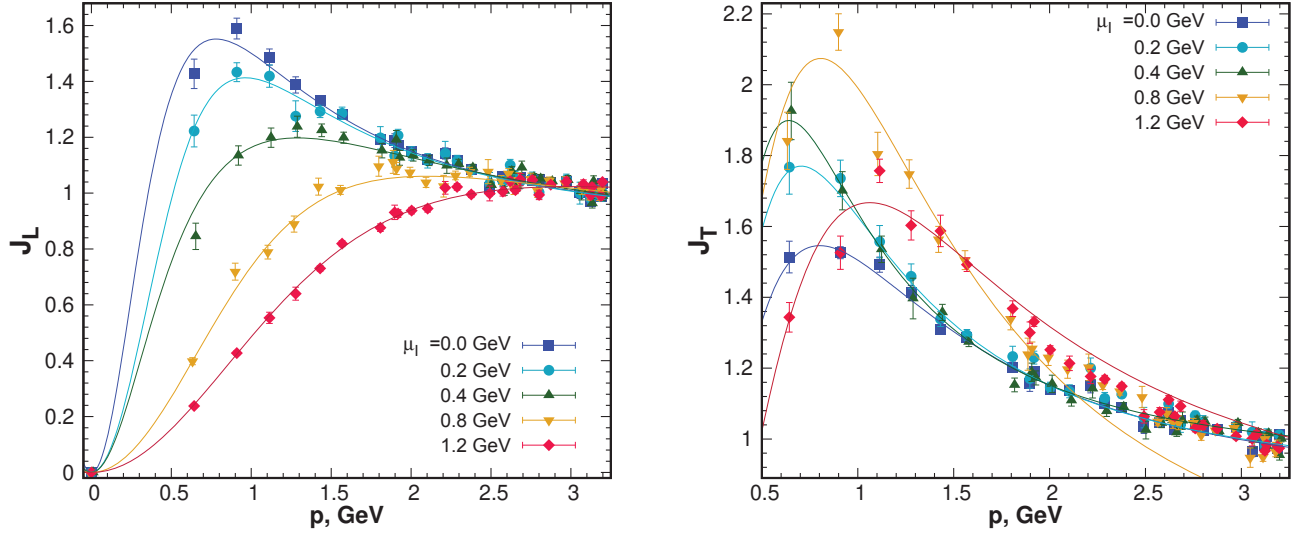


FIG. 7: The longitudinal (left) and transverse (right) gluon dressing functions at various isospin chemical potentials. The curves show results of the fit by (23).

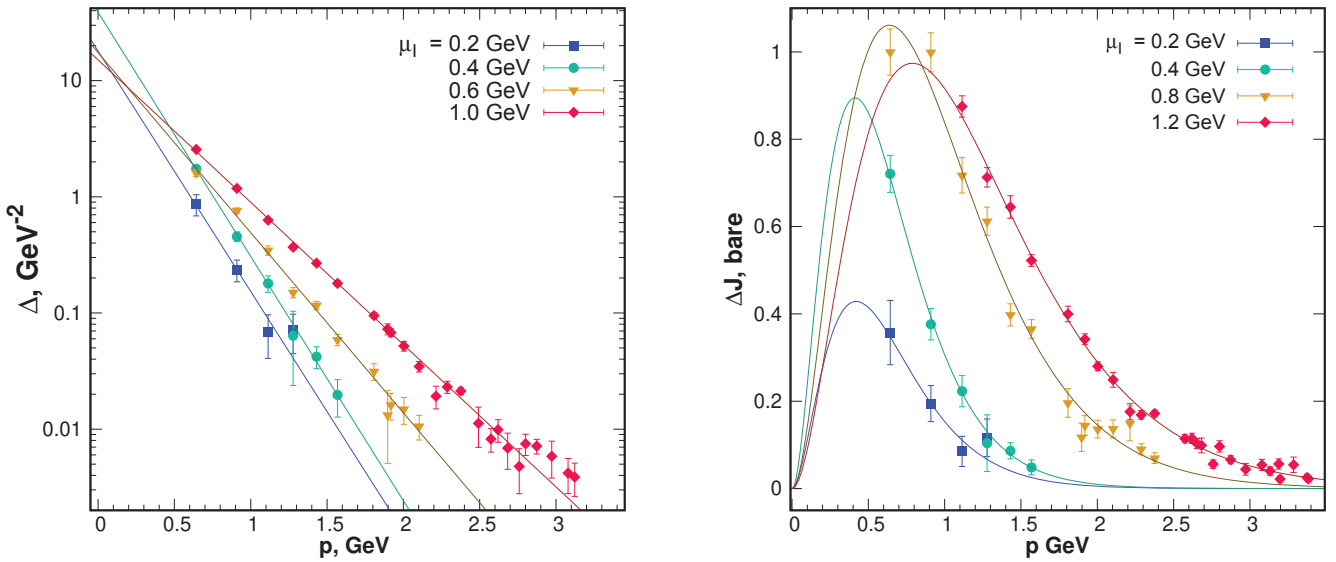


FIG. 8: The difference between the propagators $D_T - D_L$ (left) and dressing functions $J_T - J_L$ (right) as a function of the momentum. The curves show results of the fit to (27).

it also works only for $0.2 \leq \mu_I \leq 0.4$, the respective p -values as well as the fitting parameters in formula (27) are presented in Table IV. We also tried several other power-like fit functions which also have failed.

Since our data can be well approximated by the exponential function and poorly — by a power-like fit function even with 3 parameters, we arrive at the conclusion that the Gribov-Stingl fit cannot work for $D_L(p)$ and $D_T(p)$ simultaneously at large μ_I . Assuming that they do work simultaneously, we obtain the power-like dependence of the difference $D_T(p) - D_L(p)$, whereas, as we found, it cannot be fitted by a power-like func-

tion. Of course, the above reasoning is valid provided that the fit domain is sufficiently large and statistical precision is sufficiently high to discriminate between power-like and exponential behavior. Given statistical precision as in the case under consideration, power-like and exponential behavior are differentiated when the fit domain is larger than $p_{\min} \leq p < 2.2$ GeV as one can conclude from a comparison of Table IV and Fig. 8. This is the case for $\mu_I \geq 0.6$ GeV. Thus our conclusion that $\Delta(p; \mu_I) \simeq c \exp(-\nu \cdot p)$ cannot be fitted by a power-like fit function at $\mu_I \geq 0.6$ GeV agrees with the statement in Section IV that the Gribov-Stingl fit (23) for $D_T(p)$ does

not work at these values of μ_I when $p_{\text{cut}} > 2.2$ GeV, whereas the same function can be fitted well to $D_L(p)$ even at $p_{\text{cut}} = 5$ GeV for all μ_I under consideration.

We show the curves resulting from our fit (27) to $\Delta(p)$ for some values of μ_I in Fig. 8 (left panel) as well as the difference between the dressing functions

$$\Delta J(p) = p^2 \Delta(p) = J_T(p) - J_L(p) \quad (30)$$

(right panel).

The dependence of the parameters c and ν on the isospin chemical potential is shown in Fig. 9. The position and the height of the peak of the difference between the dressing functions (30) is given by the formulas

$$p_{max} = \frac{2}{\nu}, \quad \Delta J_{max} = \frac{4}{e^2} \frac{c^2}{\nu}, \quad (31)$$

the respective values are plotted in Fig. 10.

It is interesting to notice that, at $\mu_I \leq 0.4$ GeV, ΔJ_{max} rapidly increases, whereas p_{max} does not change. A completely different situation occurs at $\mu_I \geq 0.4$ GeV: ΔJ_{max} changes only slightly, whereas p_{max} increases substantially and shows a clear linear dependence on μ_I at $\mu_I \geq 0.6$ GeV. That is, the behavior of p_{max} is similar to the behavior of the electric screening mass (which is associated with the interaction radius), whereas ΔJ_{max} (which is associated with the strength of interaction) changes in an opposite manner.

VI. CONCLUSIONS

We presented first results of the study of the static longitudinal and transverse propagators in the Landau gauge of lattice QCD at nonzero isospin chemical potential.

Our main observations are as follows. We found that the longitudinal propagator $D_L(p)$ is more and more suppressed in the infrared with increasing μ_I . This is reflected, in particular, in the increase of the chromoelectric screening mass. Such dependence of $D_L(p)$ on μ_I is analogous to its dependence on temperature at $T > T_c$ [49–51]. It is also similar to dependence of $D_L(p)$ on the quark chemical potential μ_q in QC₂D [35]. We found much weaker dependence on μ_I for the transverse propagator $D_T(p)$. The question of whether the transverse propagator in the infrared domain can be adequately described in terms of screening mass may be the subject of future studies.

We determined the parameters of the Gribov-Stingl fit function (23) associated with the Gribov-Zwanziger confinement scenario. The parameters for the transverse propagator depend only weakly on μ_I and agree well with those in pure gluodynamics at $T = 0$, the parameters M_2 and M_3 for the longitudinal propagator increase with increasing μ_I . The difference between the parameters of the longitudinal and transverse propagators approaches a local peak at $\mu_I = 0.4$ GeV. This might be caused by the transition from the normal to the superfluid phase which is expected at $\mu_I \sim 0.2$ GeV.

We investigated the behavior of the dressing functions, the excess of which over one in the infrared region indicates the presence of long-range forces. At large values of μ_I the transverse dressing function is greater than the longitudinal one indicating that the chromoelectric interactions are screened at shorter distances than the chromomagnetic interactions.

Finally, we studied the difference $\Delta(p) = D_L(p) - D_T(p)$ and found that it decreases exponentially with the momentum at large p similarly to the case of the QC₂D theory [35]. We also investigated the μ_I dependence of the parameters of the exponential fit function (27) as well as the parameters p_{max} and δJ_{max} characterizing the behavior of the difference between the longitudinal and transverse dressing functions. This dependence indicates that with increasing μ_I the domain where chromomagnetic forces dominate over chromoelectric ones extends to ever shorter distances.

Our results for the gluon propagators obtained using the first principles approach of the lattice QCD should be definitely useful to test other approaches to QCD at finite isospin chemical potential like perturbation theory [32] or functional methods.

Acknowledgments. The authors are grateful to V.V. Braguta and A.Yu. Kotov for very fruitful discussions and to S.A. Sadovsky for the discussions of statistical analysis. The work was completed due to support of the Russian Foundation for Basic Research via grant 18-32-20172 mol-a-ved and grant 18-02-40130 mega. The research was carried out using the Central Linux Cluster of the NRC "Kurchatov Institute" - IHEP, the Linux Cluster of the NRC "Kurchatov Institute" - ITEP (Moscow) and the equipment of the shared research facilities of HPC computing resources at Lomonosov Moscow State University. In addition, we used computer resources of the federal collective usage center Complex for Simulation and Data Processing for Mega-science Facilities at NRC "Kurchatov Institute", <http://ckp.nrcki.ru/>.

[1] J.B. Kogut, D.K. Sinclair, Phys. Rev. D **66**, 034505 (2002)
 [2] J.B. Kogut, D.K. Sinclair, Phys. Rev. D **70**, 094501 (2004)
 [3] P. de Forcrand, M. A. Stephanov, U. Wenger, PoS **LAT-**

TICE2007, 237 (2007)
 [4] W. Detmold, K. Orginos, Z. Shi, Phys. Rev. D **86**, 054507 (2012)
 [5] P. Cea, L. Cosmai, M. D'Elia, A. Papa, F. Sanfilippo, Phys. Rev. D **85**, 094512 (2012)

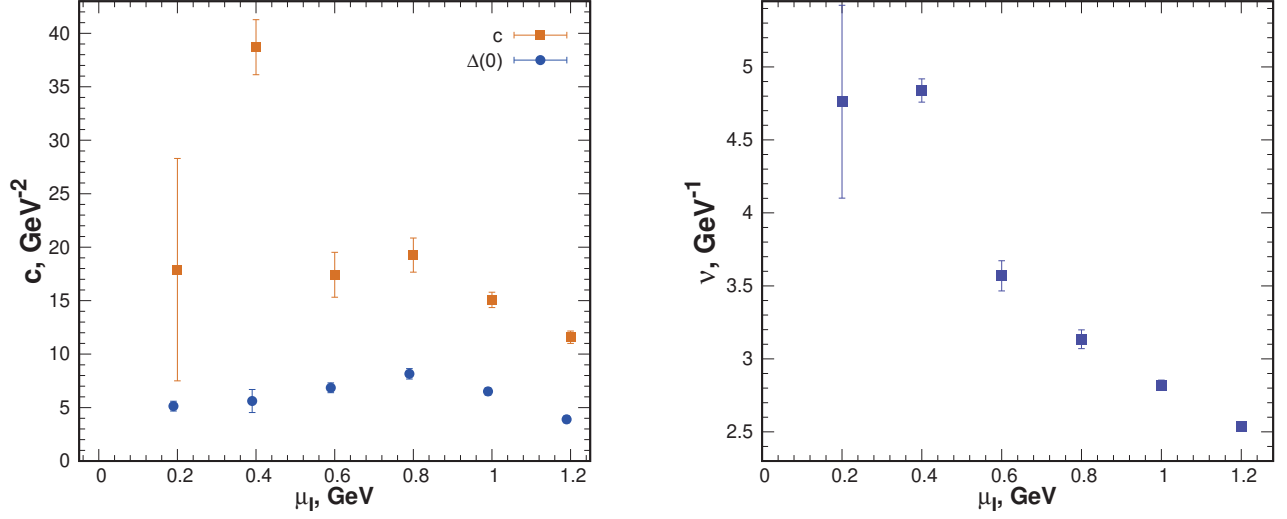


FIG. 9: The parameters of the fit function (27) as functions of μ_I . In the left panel the parameter c representing the value of $\Delta(0)$ extrapolated by formula (27) from the fit domain is compared with its actual value.

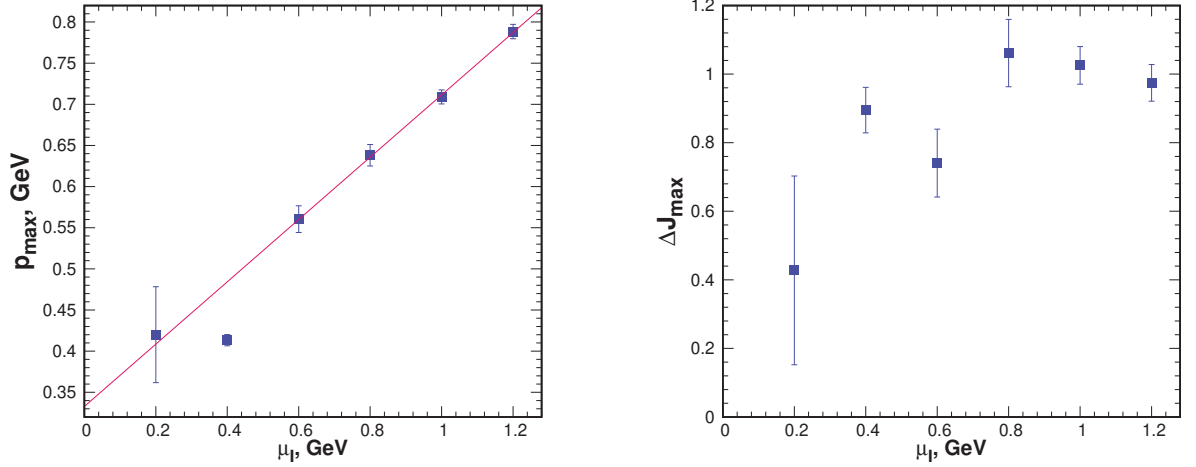


FIG. 10: Dependence of the position (left panel) and the height (right panel) of the peak of $\Delta J(p)$ on the isospin chemical potential.

- [6] G. Endrödi, Phys. Rev. D **90**, 094501 (2014)
 [7] B.B. Brandt, G. Endrodi, PoS LATTICE **2016**, 39 (2016)
 [8] B.B. Brandt, G. Endrodi, S. Schmalzbauer, Phys. Rev. D **97**, 054514 (2018)
 [9] B. B. Brandt, G. Endrodi, S. Schmalzbauer, PoS **Confinement2018**, 260 (2018)
 [10] V.V. Braguta, A.Y. Kotov, A.A. Nikolaev, JETP Lett. **110**, 1 (2019)
 [11] B.B. Brandt, F. Cuteri, G. Endrödi, S. Schmalzbauer, Particles **3**, 80 (2020)
 [12] D. Toublan, J.B. Kogut, Phys. Lett. B **564**, 212 (2003)
 [13] A. Barducci, R. Casalbuoni, G. Pettini, L. Ravagli, Phys. Rev. D **69**, 096004 (2004)
 [14] L.y. He, M. Jin, P.F. Zhuang, Phys. Rev. D **71**, 116001 (2005)
 [15] L. He, P. Zhuang, Phys. Lett. B **615**, 93 (2005)
 [16] D. Ebert, K.G. Klimenko, J. Phys. G **32**, 599 (2006)
 [17] G.F. Sun, L. He, P. Zhuang, Phys. Rev. D **75**, 096004 (2007)
 [18] T. Xia, L. He, P. Zhuang, Phys. Rev. D **88**, 056013 (2013)
 [19] T.G. Khunjua, K.G. Klimenko, R.N. Zhokhov, Phys. Rev. D **98**, 054030 (2018)
 [20] T. Khunjua, K. Klimenko, R. Zhokhov, Symmetry **11**,

- 778 (2019)
- [21] K. Kamikado, N. Strodthoff, L. von Smekal and J. Wambach, Phys. Lett. B **718**, 1044 (2013)
- [22] Z. Wang and P. Zhuang, Phys. Rev. D **96**, 014006 (2017)
- [23] P. Adhikari, J. O. Andersen and P. Kneschke, Phys. Rev. D **98**, 074016 (2018)
- [24] D. T. Son and M. A. Stephanov, Phys. Rev. Lett. **86**, 592 (2001)
- [25] K. Splittorff, D.T. Son, M.A. Stephanov, Phys. Rev. D **64**, 016003 (2001)
- [26] P. Adhikari, J.O. Andersen, Phys. Lett. B **804**, 135352 (2020)
- [27] J.O. Andersen, N. Haque, M.G. Mustafa, M. Strickland, Phys. Rev. D **93**, 054045 (2016)
- [28] T. Graf, J. Schaffner-Bielich, E.S. Fraga, Phys. Rev. D **93**, 085030 (2016)
- [29] B. Klein, D. Toublan, J.J.M. Verbaarschot, Phys. Rev. D **68**, 014009 (2003)
- [30] D. Toublan, J.B. Kogut, Phys. Lett. B **605**, 129 (2005)
- [31] M. Mannarelli, Particles **2**, 411 (2019)
- [32] T. Gorda, A. Kurkela, R. Paatelainen, S. Säppi, A. Vuorinen, 2103.05658
- [33] B.A. Freedman, L.D. McLerran, Phys. Rev. D **16**, 1130 (1977)
- [34] S. Muroya, A. Nakamura, C. Nonaka, T. Takaishi, Prog. Theor. Phys. **110**, 615 (2003)
- [35] V.G. Bornyakov, V.V. Braguta, A.A. Nikolaev, R. N. Rogalyov, Phys. Rev. D **102**, 114511 (2020)
- [36] P. Weisz, Nucl. Phys. **B212**, 1 (1983).
- [37] A. Bazavov et al., Phys. Rev. **D85**, 054503 (2012)
- [38] J.E. Mandula, M. Ogilvie, Phys. Lett. **B185**, 127 (1987).
- [39] I.L. Bogolubsky, V.G. Bornyakov, G. Burgio, E.M. Ilgenfritz, M.Muller-Preussker, V.K. Mitrjushkin, Phys. Rev. D **77**, 014504 (2008)
- [40] V.G. Bornyakov, V.K. Mitrjushkin, M. Muller-Preussker, Phys. Rev. D **81**, 054503 (2010)
- [41] J.I. Kapusta and C. Gale, *Finite-temperature field theory: Principles and applications*, (Cambridge University Press, 2011)
- [42] V. Bornyakov, A. Kotov, A. Nikolaev and R. Rogalyov, Particles **3** 308 (2020)
- [43] V.G. Bornyakov and V.K. Mitrjushkin, Int. J. Mod. Phys. A **27**, 1250050 (2012)
- [44] V.G. Bornyakov V.K. Mitrjushkin, Phys. Rev. D **84**, 094503 (2011)
- [45] O. Oliveira, P. Bicudo, J. Phys. **G38**, 045003 (2011)
- [46] P. J. Silva, O. Oliveira, P. Bicudo, N. Cardoso, Phys. Rev. **D89**, 074503 (2014)
- [47] S. Ma, *Modern Theory of critical phenomena* (W.A. Benjamin, Advanced Book Program, Minnesota University, 1976).
- [48] V.G. Bornyakov, R.N. Rogalyov, 8th International Conference on New Frontiers in Physics (2019), doi:10.1142/S0217751X20440327, 2101.01808.
- [49] A. Cucchieri, A. Maas, T. Mendes, Phys. Rev. D **75**, 076003 (2007)
- [50] C.S. Fischer, A. Maas, J.A. Muller, Eur.Phys.J. **C68**, 165 (2010)
- [51] R. Aouane, V.G. Bornyakov, E.M. Ilgenfritz, V.K. Mitrjushkin, M. Muller-Preussker, A. Sternbeck, Phys. Rev. **D85**, 034501 (2012)
- [52] D. Dudal, O. Oliveira, N. Vandersickel, Phys. Rev. **D81**, 074505 (2010)
- [53] A. Cucchieri, D. Dudal, T. Mendes, N. Vandersickel, Phys. Rev. **D85**, 094513 (2012)
- [54] O. Oliveira P.J. Silva, Phys. Rev. **D86**, 114513 (2012)
- [55] D. Dudal, O. Oliveira, P.J. Silva, Annals Phys. **397**, 351 (2018)
- [56] A. Maas, Phys. Rept. **524**, 203 (2013), 1106.3942.
- [57] M. Stingl, Z. Phys. **A353**, 423 (1996)
- [58] D. Dudal, J.A. Gracey, S.P. Sorella, N. Vandersickel, H. Vershelde, Phys. Rev. **D78**, 065047 (2008)

Appendix A: Fit results

TABLE I: Values of the parameters of the Gribov-Stingl fit (23) for the longitudinal propagator $D_L(p^2)$ at various μ_I . The cutoff momentum $p_{\text{cut}} = 5$ GeV for all values of μ_I

μ_I , GeV	$\mu_I a$	Z	M_1^2	M_2^2	M_3^4	p -value
0.0	0.000	0.864(11)	2.55(18)	0.88(11)	0.165(14)	0.26
0.2	0.070	0.865(10)	2.36(23)	0.73(15)	0.334(26)	0.56
0.4	0.139	0.826(10)	5.86(95)	3.01(58)	0.86(11)	0.28
0.6	0.209	0.838(10)	5.0(1.0)	2.41(63)	1.84(24)	0.18
0.8	0.279	0.840(10)	5.9(1.1)	2.87(60)	4.03(57)	0.89
1.0	0.348	0.840(11)	7.7(1.8)	3.95(94)	7.3(1.3)	0.15
1.2	0.418	0.819(17)	13.5(3.3)	7.2(1.5)	16.3(3.0)	0.63

TABLE II: Values of the parameters of the Gribov-Stingl fit (23) for the transverse propagator $D_T(p^2)$.

μ_I , GeV	Z	M_1^2	M_2^2	M_3^4	p -value	p_{cut} , GeV
0.0	0.837(8)	2.96(16)	1.02(10)	0.189(11)	0.47	5.0
0.2	0.861(8)	2.01(14)	0.47(9)	0.125(9)	0.04	5.0
0.4	0.914(9)	1.36(14)	0.23(6)	0.087(8)	0.91	3.0
0.6	0.687(7)	4.7(1.3)	1.05(28)	0.259(47)	0.68	2.2
0.8	0.473(5)	8.9(4.9)	1.03(40)	0.326(79)	0.08	2.2
1.0	0.619(7)	6.4(2.4)	1.07(34)	0.381(78)	0.18	2.2
1.2	0.724(11)	6.2(5.0)	1.40(92)	0.72(31)	0.05	1.9

TABLE III: Dependence of the parameters M_i , determined by a fit of the formula (23) to $D_L(p)$ over the range $0 \leq p < p_{\text{cut}}$ on the cutoff momentum p_{cut} at $\mu_I = 0$.

p_{cut} , GeV	M_1^2	M_2^2	M_3^4	p -value
2.2	3.59(83)	1.20(27)	0.214(36)	0.92
2.6	2.67(50)	0.90(20)	0.172(26)	0.74
3.0	2.04(23)	0.67(11)	0.139(14)	0.86
3.5	2.10(18)	0.69(10)	0.143(13)	0.70
4.0	2.26(18)	0.75(11)	0.151(13)	0.39
4.5	2.43(19)	0.82(12)	0.159(14)	0.20
5.0	2.55(18)	0.88(12)	0.165(14)	0.25

TABLE IV: Parameters c and ν as well as ΔJ_{max} determined by fitting formula (27) to our data for $\Delta(p)$. In the last two columns the values of the goodness-of-fit parameter corresponding to (27) and (29) are compared.

μ_I	p_{cut} , GeV	c , GeV $^{-2}$	ν , GeV $^{-1}$	ΔJ_{max}	p -value eq.(27)	p -value eq.(29)
0.2	1.3	17.9(10.4)	4.76(66)	0.52(21)	0.39	0.57
0.4	1.6	38.7(5.0)	4.839(80)	0.91(13)	0.96	0.43
0.6	2.2	17.4(2.1)	3.57(10)	0.738(76)	0.086	0.002
0.8	2.5	19.3(1.6)	3.135(64)	1.066(65)	0.056	0.0004
1.0	3.1	15.07(72)	2.821(54)	1.014(64)	0.039	10^{-8}
1.2	3.4	11.58(58)	2.537(28)	0.978(49)	0.067	0